Branching of center vortices in SU(3) lattice gauge theory

Felix Spengler, Markus Quandt, and Hugo Reinhardt
Institut für Theoretische Physik, Auf der Morgenstelle 14, D-72076 Tübingen, Germany

(Received 9 October 2018; published 16 November 2018)

We analyze the branching of center vortices in SU(3) Yang-Mills theory in maximal center gauge. When properly normalized, we can define a branching probability that turns out to be independent of the lattice spacing (in the limited scaling window studied here). The branching probability shows a rapid change at the deconfinement phase transition, which is much more pronounced in space slices of the lattice as compared to time slices. Though not a strict order parameter (in the sense that it vanishes in one phase) the branching probability is thus found to be a reliable indicator for both the location of the critical temperature and the geometric rearrangement of vortex matter across the deconfinement phase transition.

DOI: 10.1103/PhysRevD.98.094508

I. INTRODUCTION

The center vortex picture is one of the most intuitive and prolific explanations of color confinement in strong interactions. It was first proposed by Mack and Petkova [1], but lay dormant until the advent of new gauge fixing techniques that permitted the detection of center vortex structures directly within lattice Yang-Mills configurations [2]. These numerical studies have revealed a large amount of evidence in favor of a center vortex picture of confinement: The center vortex density detected on the lattice in the maximal center gauge after center projection properly scales with the lattice constant in the continuum limit, and therefore, it must be considered a physical quantity [3]. When center vortices are removed from the ensemble of gauge field configurations the string tension is lost in the temporal Wilson loop. Conversely, keeping the center vortex configurations only, the static quark potential extracted from the temporal Wilson loop is linearly rising at all distances [2]. Center vortices also seem to carry the nontrivial topological content of gauge fields: the Pontryagin index can be understood as the self-intersection number of center vortex sheets in four Euclidean dimensions [4,5], or in terms of the writhing number of their three-dimensional (3D) projection, which are loops [5]. For the color group SU(2), attempts to restore the structure of the underlying (fat) vortices suggest that the topological charge also receives contributions from the color structure of self-intersection regions of such fat vortices [6,7]. Removing the center vortex content of the gauge fields makes the field configuration topologically trivial and simultaneously restores chiral symmetry. The Pontryagin index [8], as well as the quark condensate [9,10], are both lost when the center vortices are removed, see also [11]. In the case of SU(3), this link of center vortices to both confinement and chiral symmetry breaking has also been observed directly in lattice simulations of the low lying hadron spectrum [12]. Finally, the center vortex picture also gives a natural explanation of the deconfinement phase transition, which appears as a depercolation transition from a confined phase of percolating vortices to a smoothly interacting gas of small vortices winding dominantly around the compactified Euclidean time axis [13].

Center vortices detected on the lattice after center projection form loops in $D = 3$ dimensions and surfaces in $D = 4$; in both cases, they live on the *dual* lattice and are closed due to Bianchi's identity. While a gas of closed loops can be treated analytically, see e.g., [14], an ensemble of closed sheets is described by string theory, which has to be treated numerically. The main features of $D = 4$ center vortices detected on the lattice after center projection, such as the emergence of the string tension or the order of the deconfinement transition, can all be reproduced in an effective *random center vortex model*: in this approach, vortices are described on a rather coarse dual lattice (to account for the finite vortex thickness), with the action given by the vortex area (Nambu-Goto term), plus a penalty for the curvature of the vortex sheets to account for vortex stiffness [15–17]. The model was originally formulated for the gauge group SU(2) [15] and later extended to SU(3) in Ref. [16].

The SU(3) group has two nontrivial center elements $z_{1/2} = e^{\pm i2\pi/3}$ that are related by $z_1^2 = z_2$, $z_2^2 = z_1$. Because

of this property, two z_1 center vortices can fuse to a single z_2 vortex sheet and vice versa (see Fig. 2 below). This vortex branching is a new element absent in the gauge group SU(2). In Ref. [16], it was found within the random center vortex model that the deconfinement phase transition is accompanied with a strong reduction of the vortex branching and fusion. In the present paper, we investigate the branching of center projected lattice vortices found in the maximal center gauge.

This paper is organized as follows: In Sec. II, we describe the geometrical and physical properties of vortex branching and develop the necessary quantities to study this new phenomenon on the lattice. Section III gives details on our numerical setup and the lattice parameters and techniques used in the simulations. The results are presented and discussed in Sec. IV, and we close with a short summary and an outlook to future investigations.

II. CENTER VORTEX BRANCHING POINTS

On the lattice, center vortices are detected by first fixing all links $U_\mu(x)$ to a suitable center gauge, preferably the so-called *maximal center gauge* (MCG), cf. Eq. (4) below. This condition attempts to find a gauge transformation that brings each link, on average, as close as possible to a center element. The transformed links are then projected on the nearest center element, $U_\mu(x) \to Z_\mu(x) \in \mathbb{Z}_N$, and since it was already close, we can hope that the resulting $\mathbb{Z}_N$ theory preserves the relevant features of the original Yang-Mills theory. In fact, it has been shown that the string tension is retained to almost 100% under the center projection for the color group $G = \mathrm{SU}(2)$ and still to about 62% for $G = \mathrm{SU}(3)$ [18], while the string tension disappears for all G if vortices are removed [2,19]. Also, the near-zero modes of the Dirac operator relevant for chiral symmetry breaking disappear if vortices are removed from the physical ensemble [9,10].

The center projected theory is much simpler to analyze. Since all links are center valued after projection, so are the plaquettes. If such a center-valued plaquette happens to be nontrivial, it is said to be pierced by a center vortex, i.e., the corresponding *dual* plaquette is considered part of a center vortex world sheet. For $G = \mathrm{SU}(3)$, in particular, we associate a center projected plaquette $Z_{\mu\nu}(x)$ in the original lattice with a *triality* $q_{\alpha\beta}(x^*) \in \{0, 1, 2\}$ on the dual lattice, where

$$Z_{\mu\nu}(x) = \exp\left[i\frac{\pi}{3}\epsilon_{\mu\nu\alpha\beta}q_{\alpha\beta}(x^*)\right]. \tag{1}$$

Here, the usual sum convention over greek indices is in effect, and the footpoint of the dual plaquette is defined as $x^* = x + (\mathbf{e}_\mu + \mathbf{e}_\nu - \mathbf{e}_\alpha - \mathbf{e}_\beta)/2$. As the reader may convince herself, this assignment is such that the initial and dual plaquette link with each other. The triality can be viewed as a quantized flux of field strength flowing through the original plaquette. It is, however, only defined modulo $N = 3$, so that a $q = 1$ vortex is equivalent to $q = -2$, which in turn is a $q = 2$ vortex with an opposite direction of flux. This ambiguity gives rise to different geometrical interpretations (see. Fig. 2), but it does not affect the quantities studied in the present work. The vortex world sheet itself is now composed of all connected nontrivial dual plaquettes. This world sheet may *branch* along links of the dual lattice where three or more vortex plaquettes join, cf. the left panel of Fig. 1.

For the actual measurement, we study the branching in the original lattice, where the branching link is dual to an elementary cube, while the plaquettes attached to the branching link are dual to the plaquettes on the surface

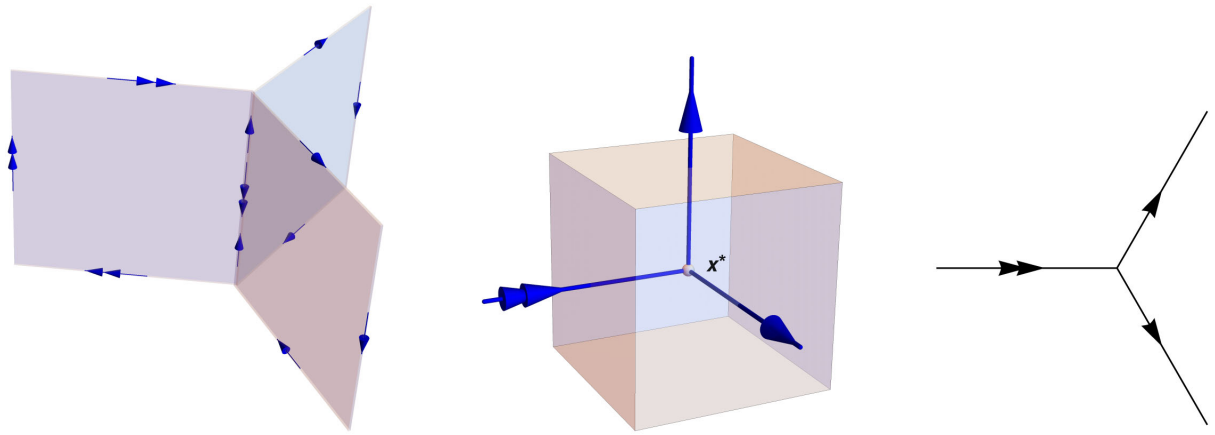

FIG. 1. Illustration of vortex branching. The single and double arrows on the lines represent triality $q = 1$ and $q = 2$, respectively. The left figure represents a $\nu = 3$ vortex branching in the full 4D lattice. The graphic in the middle shows the same situation from a 3D slice, where the vortex plaquettes are replaced by three flux tubes joining at a branching point x^*. The tubes enter the elementary cube surrounding x^* by piercing three of its six surface plaquettes. The right figure gives a simplified picture where only the branching vortex lines are displayed.

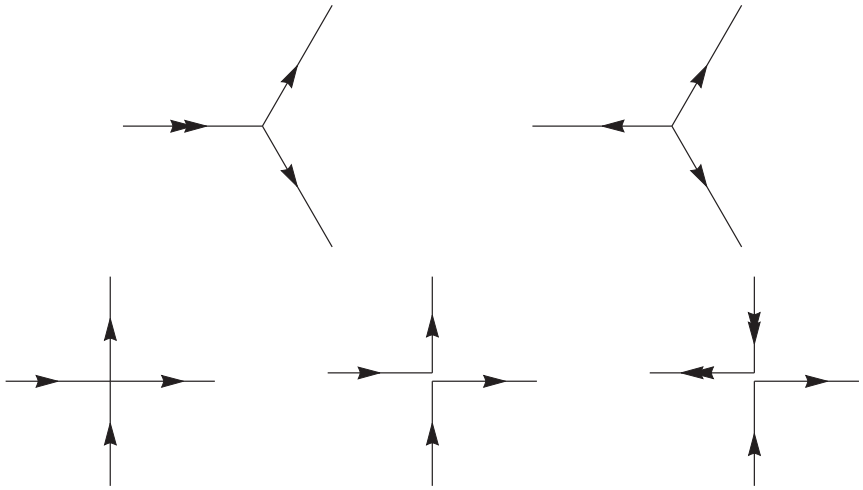

FIG. 2. Ambiguities in the interpretation of SU(3) vortex branching. In the top line, the simple branching of a $q = 2$ vortex on the left can be equivalently described as three $q = 1$ vortices emanating from a common source, i.e., as the $\mathbb{Z}_3$ center monopole. Similarly, the self-intersection of a $q = 1$ vortex in the bottom line (left), is equivalent to an osculation point of, e.g., two $q = 1$ vortices (middle) or a $q = 1$ and a $q = 2$ vortex (right).

of the cube. Geometrically, this can be visualized in the 3D slice[1] of the original lattice that contains the cube, cf. Fig. 1: in this slice, the vortex plaquettes are projected onto links that are dual to the nontrivial plaquettes and represent the center flux through the plaquettes. Vortex matter thus appears as a network of closed lines composed of nontrivial dual links. These thin lines are the projection vortices in which the center flux of the unprojected (thick) vortex is compressed into a narrow tube with a cross section of only a single plaquette.

Vortex branching in a 3D slice occurs at *branching points*, which are the projection of the branching links in the 4D lattice. Geometrically, the branching points are located in the middle of the cubes dual to the branching links as illustrated in Fig. 1: the vortex lines entering an elementary cube must pierce the plaquettes on its surface, and up to six vortices can join at any given point of the dual 3D slice.[2] We call this number $\nu(x^*) \in \{0, \ldots, 6\}$ of vortex lines joining at a site x^* of the dual 3D slice its *branching genus*. Clearly, $\nu = 0$ means that no vortex passes through x^*, while $\nu = 2$ means that a vortex goes in and out without branching (but possibly changing its direction). The cases $\nu = 4$ and $\nu = 6$ correspond to vortex self-intersections (or osculation points), which are also present in the case of $G = \mathrm{SU}(2)$. The odd numbers $\nu = 3$ and $\nu = 5$, however, are genuine vortex branchings that cannot be observed in SU(2), and they are thus a new feature of the center projected theory for the more complex color group SU(3). In the present study, we investigate the distribution of branching points in 3D slices across the deconfinement phase transition.

It should also be mentioned that the case $\nu = 1$ would represent a vortex end point, which is forbidden by Bianchi's identity, i.e., flux conservation modulo 3. More precisely, Bianchi's identity in the present case states that the sum of the trialities of all plaquettes in an elementary cube of a 3D slice must vanish modulo N (the number of colors). This holds even for cubes on the edge of the lattice if periodic boundary conditions are employed. Clearly, this rule is violated if the cube has only $\nu = 1$ nontrivial plaquette, which is hence forbidden. In our numerical study, the number of $\nu = 1$ branching points must then be exactly zero, which is a good test on our algorithmical bookkeeping.

Finally, we must also stress that $\nu = 6$ branchings for the color group $G = \mathrm{SU}(2)$ are *always* self-intersections or osculation points, while they can also be interpreted as *double vortex branchings* in the case of $G = \mathrm{SU}(3)$. With the present technique, we cannot keep track of the

TABLE I. Possible vortex branching types and their geometrical interpretation. As explained in Fig. 2, there is some arbitrariness in the geometrical picture, while the branching genus ν is independent of all conventions.

$\nu = 0$	no vortex
$\nu = 1$	vortex end point, forbidden by Bianchi's identity
$\nu = 2$	nonbranching vortex
$\nu = 3$	simple vortex branching
$\nu = 4$	vortex self-intersection/osculation
$\nu = 5$	complex vortex branching
$\nu = 6$	complex vortex self-intersection/osculation/double branching

[1]Such slices are obtained by holding either the Euclidean time coordinate x_0 (*time slice*) or a space coordinate x_i (*space slice*) fixed.

[2]Equivalently, up to six vortex plaquettes in $D = 4$ can join a common branching link.

TABLE II. Parameters for the finite temperature simulations. The last row gives the number of configurations used for measurements, and the spatial lattice size was $L_s = 24$ in all cases.

β	5.8					5.85					5.9				
L_t	3	4	5	6	9	4	5	6	7	10	4	5	6	7	10
# configs	140	102	106	90	92	122	98	80	73	73	119	107	75	74	78

orientation of vortices (i.e., the direction of the vortex flux), and hence, we are unable to distinguish double branchings from complex self-intersections. Fortunately, $\nu = 6$ branching points are so extremely rare that they can be neglected entirely for our numerical analysis. If we speak of vortex branching, we thus always mean the cases $\nu = 3$ and $\nu = 5$, which only exist for $G = \mathrm{SU}(3)$, and for which all possible interpretations involve a single vortex branching. Table I summarizes again the different sorts of vortex branchings and their geometrical meaning.

III. NUMERICAL SETUP

We simulate SU(3) Yang-Mills theory on a hypercubic lattice using the standard Wilson action as a sum over all plaquettes $U_P \equiv U_{\mu\nu}(x)$

$$S = \sum_P \left[1 - \frac{1}{2N}\mathrm{tr}(U_P + U_P^\dagger)\right]. \tag{2}$$

Configurations are updated with the pseudoheatbath algorithm due to Cabibbo and Marinari [20] applied to a full set of SU(2) subgroups. To study finite temperature, we reduce the extent L_t of the Euclidean time direction, while keeping the spatial extent $L_s \gg L_t$ to eliminate possible finite size effects,

$$T = \frac{1}{a(\beta)L_t}. \tag{3}$$

Since the variation of L_t only allows for a rather coarse temperature grid, we have also varied the lattice spacing $a(\beta)$ by considering three different couplings β within the scaling window.[3] Table II lists the lattice extents and coupling constants used in our simulations.

For each run, the lattice was thermalized using at least 100 heatbath sweeps, and measurements were then taken on 70 to 200 thermalized configurations (depending on L_t), with 10 sweeps between measurements to reduce autocorrelations. For each measurement, the following sequence of steps was performed:

(a) *Gauge fixing to the maximal center gauge:* This is achieved by maximizing the functional

$$F = \frac{1}{V}\sum_{\{x,\mu\}}\left|\frac{1}{N}\mathrm{tr}U_\mu(x)\right|^2, \tag{4}$$

under gauge rotations, where $N = 3$ is the number of colors and $V = \prod_\mu L_\mu$ is the lattice volume. The main gauge fixing algorithm used in this study is the iterated overrelaxation [21] in which the local quantity

$$F_x = \sum_\mu (|\mathrm{tr}\{\Omega(x)U_\mu(x)\}|^2 + |\mathrm{tr}\{U_\mu(x-\hat{\mu})\Omega^\dagger(x)\}|^2) \tag{5}$$

is maximized with respect to a local gauge rotation $\Omega(x) \in \mathrm{SU}(3)$ at each lattice site x. We stop this process when the largest relative change of F_x at all sites x falls below 10^{-6}. More advanced gauge fixing techniques, such as simulated annealing [22] or Landau gauge preconditioners [23] from multiple random initial gauge copies, have also been tested. While such methods are known to have a significant effects on the propagators of the theory in any gauge [24,25], we found that they have very little effect, at our lattice sizes, on the gauge fixing functional and the vortex geometry investigated here. For the production runs, we have therefore reverted to simple overrelaxation with random starts.

(b) *Center projection:* Once a configuration is fixed to the MCG, each link is projected to its closest center element $U_\mu(x) \to Z_\mu(x)$ by first splitting off the phase

$$\mathrm{tr}U_\mu(x) = |\mathrm{tr}U_\mu(x)| \cdot e^{2\pi i \delta_\mu/N}, \tag{6}$$

which defines $\delta_\mu \in \mathbb{R}$ modulo N. After rounding (δ_μ mod N) to the closest integer $q_\mu \in [0, N-1]$, we can then extract the center projected link as

$$Z_\mu(x) \equiv \exp\left(i\frac{2\pi}{N}q_\mu\right)\mathbb{1} \in \mathbb{Z}_N. \tag{7}$$

In the case of SU(3), we will call the integer $q_\mu \in \{0,1,2\}$ the *triality* of a center element. As mentioned earlier, the triality is only defined modulo 3, i.e., $q_\mu = -2$ is identical to $q_\mu = 1$. While this ambiguity alters the geometric interpretation of a given vortex distribution (cf. Fig. 2), both the existence of a vortex branching point and its genus (the number of vortex lines meeting at the point) are independent of the triality assignment.

[3]Finer temperature resolutions through the use of anisotropic lattices proved to be unnecessary for the present investigation.

(c) *Vortex identification:* After the center projection, all links are center valued, and so are the projected plaquettes. If such a center-valued plaquette happens to be nontrivial, we interpret this as a center vortex piercing the plaquette, i.e., the corresponding dual plaquette is part of the center vortex world sheet. The exact formula for the triality assignment of the vortex plaquettes was given in Eq. (1) above. For the computation of the area density of vortices, it is sufficient to consider a 2D plane in the original lattice and count the number of nontrivial plaquettes after center projection.

(d) *branching points:* As explained earlier, center vortices appear within a time or space slice as a network of links on the lattice dual to the slice. At each point x^* of this dual 3D slice, between $\nu = 0, 2, \ldots, 6$ vortex lines may join. Since the point x^* is the center of an elementary cube of the original time or space slice, the vortices joining in x^* must enter or exit the cube and hence pierce some or all of the six plaquettes on its surface. We can thus determine $\nu(x^*)$ simply by counting the number of nontrivial plaquettes on elementary cubes in 3D slices of the lattice, and we assign it to the possible branching point x^* in the middle of the cube.

IV. RESULTS

The vortex area density is known to be a physical quantity in the sense that it scales properly with the lattice spacing $a(\beta)$ (see below) [3]. This entails that the overall amount of vortex matter quickly decays with increasing coupling β. To improve the statistics, we therefore choose coupling constants β near the lower end of the scaling window $5.7 \lesssim \beta \lesssim 7$, cf. Table II. Since this implies a rather coarse lattice, we must ensure that the lattice size in the short time direction does not become too small. For the values of β chosen in our simulation, $L_t = [a(\beta)T]^{-1} \gg 1$ for temperatures at least up to $T \lesssim 2T^*$, which is entirely sufficient for the present purpose. We have also checked that increasing the spatial volume from $L_s = 16$ to $L_s = 24$ has only marginal effects on the results, so that finite volume errors are also under control. In the final results, we only include the findings for the larger lattice extent $L_s = 24$.

The properties of vortex matter are intimately related to the choice and implementation of the gauge condition, as well as the absence of lattice artifacts. In particular, the vortex area density only survives the continuum limit if MCG is chosen and implemented accurately, and the lattice spacing is sufficiently small to suppress artifacts. As an independent test of these conditions, we have therefore reanalyzed the area density ρ of vortex matter. In lattice units, this is defined as the ratio

$$\hat{\rho}(\beta) = a(\beta)^2\rho = \frac{\#\text{nontrivial center plaquettes}}{\#\text{total plaquettes}} \quad (8)$$

in every 2D plane within the lattice. (We average over all planes in the full lattice, or in appropriate 3D slices, in order to improve the statistics.) After gauge fixing and center projection, the measurement of the vortex density is therefore a simple matter of counting nontrivial plaquettes. If we assume that the vortex area density is a physical quantity that survives the continuum limit, we should have $\rho = c\sigma$, where σ is the physical string tension and c is a dimensionless numerical constant. A random vortex scenario [1] entails $\sigma = \frac{3}{2}\rho$ for $G = \mathrm{SU}(3)$, which corresponds to $c = 0.67$. Previous lattice studies found a somewhat smaller value of about $c = 0.5$ instead, indicating that the random vortex picture for MCG vortices at $T = 0$ is not always justified [18]. In lattice units, these findings translate into

$$\frac{\hat{\rho}(\beta)}{\hat{\sigma}(\beta)} = \frac{a(\beta)^2\rho}{a(\beta)^2\sigma} = \frac{\rho}{\sigma} = c \simeq 0.5 \quad \text{independent of } \beta \text{ in the scaling window.} \quad (9)$$

For our values of the coupling, as in Table II, we have not measured the area density $\hat{\rho}(\beta)$ at $T = 0$ directly, but instead, we took the data from the largest temporal extent $L_t = 10$ that corresponds to a temperature $T/T^* \approx 0.55$ deep within the confined phase. Since the string tension and the vortex density do not change significantly until very close to the phase transition, the $L_t = 10$ data should still be indicative for the values at $T = 0$. From these results and the string tension data $\hat{\sigma}(\beta)$ in Ref. [26], the ratio (9) can then be determined as follows:

β	5.8	5.85	5.9
c	0.558	0.573	0.591

As can be seen from this chart, the ratio (9) is indeed roughly constant in the considered coupling range, and it is also in fair agreement with previous lattice studies [18], given the fact that we did not really make a $T = 0$ simulation. In addition, inadequately gauge fixed configurations would show increased randomness, which would lead to a significant drop in the vortex density as compared to the string tension data from Ref. [26], and hence a much smaller value of c. We thus conclude that our chosen lattice setup and gauge fixing algorithm are sufficient for the present investigation.

Next, we study the finite temperature behavior of vortex matter. The critical deconfinement temperature for $G = \mathrm{SU}(3)$ is given by $T^*/\sqrt{\sigma} \approx 0.64$ [26]. Since we do not measure the string tension independently, we can use Eq. (9)

$$\frac{T^*}{\sqrt{\rho_0}} = \frac{T^*}{\sqrt{\sigma}}\sqrt{\frac{\sigma}{\rho_0}} = \frac{T^*/\sqrt{\sigma}}{\sqrt{c}} \approx 0.90 \quad (10)$$

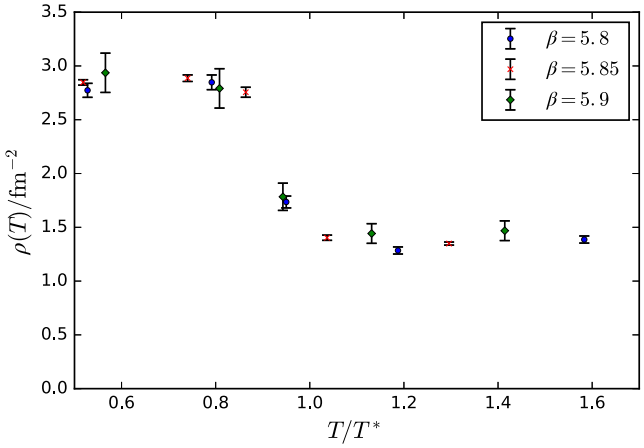

FIG. 3. Vortex area density near the phase transition.

to determine the critical temperature in units of the zero-temperature vortex density $\rho_0 \equiv \rho(T = 0)$, which sets the scale in our simulations. In absolute units,

$$\sqrt{\rho_0} = \sqrt{c\sigma} \approx 330 \text{ MeV}. \tag{11}$$

From the results in Fig. 3, we see that there is roughly a 50% drop in the vortex density at the critical temperature, which is consistent with the findings of Ref. [18]. A complete loss of vortex matter at T^* would mean that both the temporal *and* spatial string tension would vanish in the deconfined phase, contrary to lattice results [27]. What happens instead is a *percolation phase transition* in which the geometric arrangement of vortices changes from a mostly random ensemble to a configuration in which most vortices are aligned along the short time direction [13]. Since this leads to a nearly vanishing vortex density in space slices while the average density only drops mildly, the density in time slices and the associated spatial string tension must even increase for $T > T^*$.

These considerations imply that a good order parameter for confinement in the vortex picture should be sensitive to the randomness or order in the geometric arrangement of vortex matter and, as a consequence, should behave differently in temporal or spatial 3D slices of the lattice. A prime candidate in SU(3) Yang-Mills theory is the three-volume density of *branching points*, since it is directly defined in 3D slices and describes deviations of the vortex cluster from a straight aligned ensemble. This has previously been studied in the effective center vortex model [16], where indeed a significant drop of vortex branching was observed in the deconfined phase, but not directly in lattice Yang-Mills theory.

Since vortex branching implies a deviation from a straight vortex flow, we expect that it is suppressed in the deconfined phase where most vortices wind directly around the short time direction. In addition, the residual branching for $T > T^*$ should be predominantly in a space direction (since the vortices are already temporally aligned) and should hence be mostly visible in *time slices*, where the vortex matter is expected to still form large percolating clusters. In space slices, by contrast, vortices are mostly aligned (along the time axis) in the deconfined phase, and the suppression of the remnant branching for $T > T^*$ should be much more pronounced.

To test these expectations, we have measured the (dimensionless) volume density of branching points

$$\hat{\rho}_B \equiv \frac{\text{branching points in lattice dual to 3D slice}}{\text{total sites in lattice dual to 3D slice}} = \frac{\text{elementary cubes in 3D slice with } v \in \{3,5\}}{\text{all elementary cubes in 3D slice}}, \tag{12}$$

by assigning the vortex genus $\nu \in \{0, \ldots, 6\}$ to all elementary cubes in a 3D slice, cf. Sec. II, and counting them. (To improve the statistics, we have averaged over space and time slices separately, using the same thermalized configurations.) Generally, we find:

(1) Vortex endpoints with $\nu = 1$ do not appear, i.e., vortices are closed in accordance with Bianchi's identity.
(2) Vortex branchings are rare as compared to $\nu = 2$ nonbranching vortex matter.
(3) Complex vortex branchings with $\nu = 5$ are very rare and significantly reduced as compared to the simple branchings with $\nu = 3$; numerically, the $\nu = 5$ branchings contribute with only 0.1…1.0% to the total branching probability.

To construct a quantity that has the chance of scaling to the continuum, we must express the branching density in physical units,

$$\rho_B(T, \beta) \equiv \frac{\hat{\rho}_B(T, \beta)}{a(\beta)^3}, \tag{13}$$

where $a(\beta)$ is the lattice spacing at coupling β, which we take from Ref. [26]. Equation (13) is indeed a physical quantity, as can be seen directly from the result in Fig. 4, where the data for all β considered here fall on a common curve. Since we only considered a limited range of couplings β, one could be worried that possible scaling violations in ρ_B would not be very pronounced. As can be seen from the right panel of Fig. 4, this is not the case. The dimensionless density (12), for instance, exhibits large scaling violations that are clearly visible even for our restricted range of couplings. This gives a strong indication that the branching density $\rho_B(T)$ really survives the continuum limit, even though further simulations at large couplings would be helpful to corroborate this fact.

From Fig. 5, the physical branching density indeed shows a rapid drop at the critical temperature $T = T^*$, while it stays roughly constant below and above T^*. In particular, the maximal value is expected at $T \to 0$.

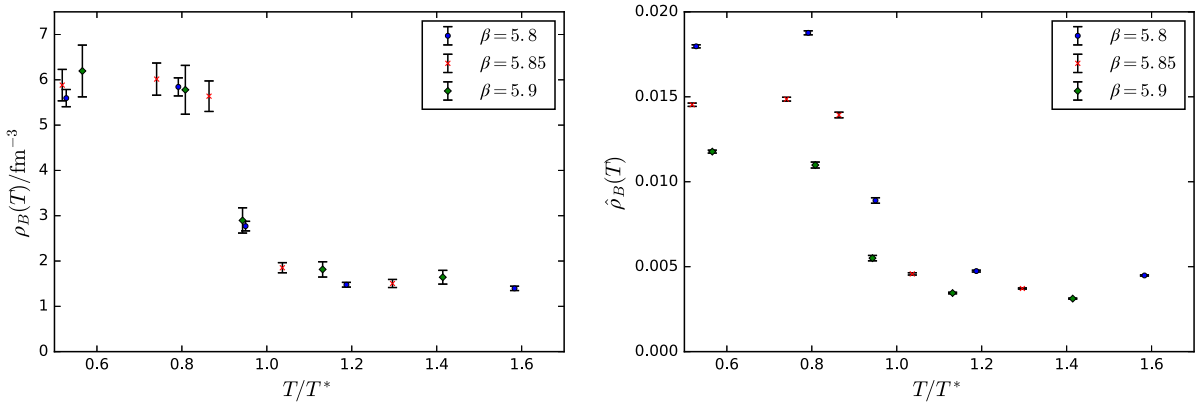

FIG. 4. Scaling of the volume density of vortex branching in space slices of the lattice. The physical density (13) (*left*) shows no apparent scaling violations. For comparison, the dimensionless density (12) (*right*) shows the amount of scaling violations to be expected for the present range of couplings. Error bars for the physical density are much larger since they also include uncertainties in the physical scale taken from Ref. [26].

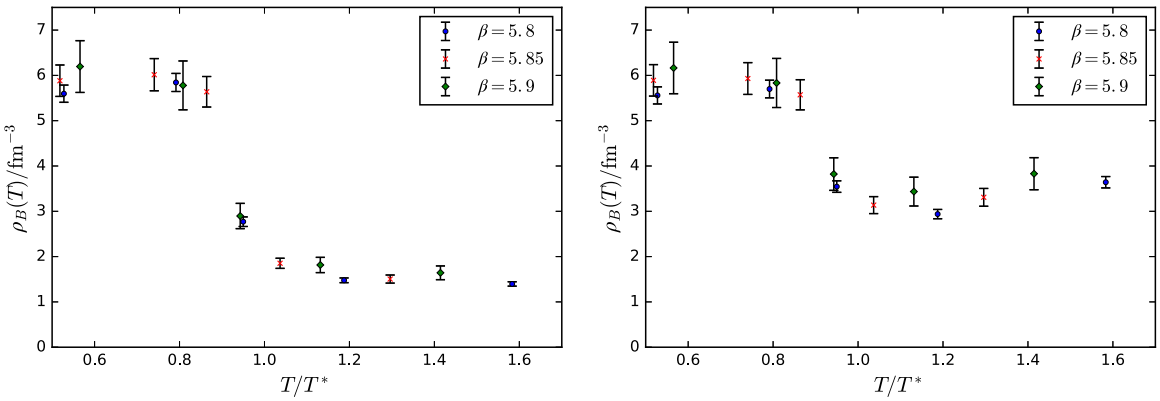

FIG. 5. Volume density of vortex branching points in physical units, measured in space slices (*left*) and time slices (*right*). Error bars include statistical errors and uncertainties in the physical scale taken from Ref. [26].

We have not made independent measurements at $T = 0$, but the available data from $L_t = 9$ and $L_t = 10$ corresponding to $T/T^* = 0.55$ should still be indicative for the value at zero temperature, since the vortex properties are known to show no significant change until very close to the phase transition. With this assumption, we find, in absolute units,

$$\rho_B(0) \approx 5.86\ \mathrm{fm}^{-3} = (0.56\ \mathrm{fm})^{-3}. \tag{14}$$

There is also a remnant branching density in the deconfined phase, but this is much smaller in space slices [20% of $\rho_B(0)$] than in time slices (60%), in agreement with our geometrical discussion of vortex branching above. In fact, the branching density in time slices even increases slightly with the temperature within the deconfined phase.

Next, we want to demonstrate that the steep drop in the branching density is *not* due to an overall reduction of vortex matter itself, but rather it signals a geometrical rearrangement. Instead of studying ρ_B/ρ directly, we make a small detour and first introduce the *branching probability*

$$q_B \equiv \frac{\#\text{ elementary cubes in 3D slice with } \nu \in \{3,5\}}{\#\text{ all elementary cubes in 3D slice with } \nu \neq 0}, \tag{15}$$

which gives the likelihood that a vortex that enters an elementary cube of edge length equal to the lattice spacing $a(\beta)$ will actually branch within that cube. The branching probability q_B itself cannot be a physical quantity since it is expected to be proportional to the lattice spacing a near the continuum limit.[4] This entails that the *branching probability per unit length*

[4]To see this, assume that the probability of branching in a cube of edge length $a \ll 1$ is $q \ll 1$, and consider a cube of length na composed of n^3 subcubes of length a. Since vortices are stiff, most nonbranching vortices do not change their direction if $a \ll 1$ and just pass straight through n subcubes. The probability of nonbranching within the na cube is therefore $(1-q)^n$ at small spacing, so that the branching probability in the na cube becomes $1-(1-q)^n \approx nq$, i.e., it is proportional to the edge length of the cube.

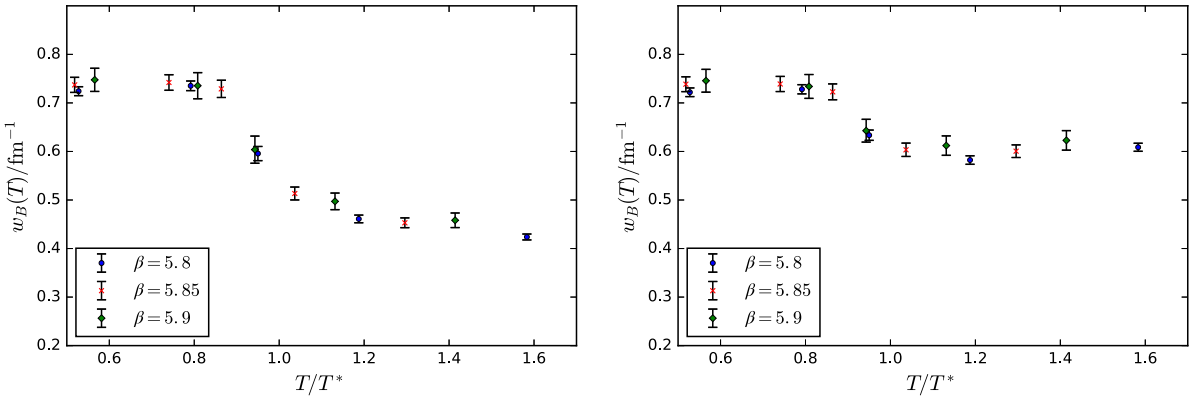

FIG. 6. Branching probability per unit length (16) in physical units, measured in space slices (*left*) and time slices (*right*). Error bars include statistical errors and uncertainties in the physical scale taken from Ref. [26].

$$w_B(T,\beta) \equiv \frac{q_B(T,\beta)}{a(\beta)} \tag{16}$$

could be a physical quantity. As can be seen from Fig. 6, this is indeed the case as the curves for w_B for all available couplings fall on a common curve. The temperature dependence of the physical quantity $w_B(T)$ is very similar to the branching density in Fig. 4, with the drop at $T = T^*$ being reduced from 75% to about 50%. The qualitative features of the branching probability per unit length are, however, very similar to the branching point density, and both are physical quantities that scale to the continuum.

Next we want to show that the branching probability per unit length w_B is actually related to the ratio ρ_B/ρ of branching points and vortex matter density. To see this, we consider an arbitrary 3D slice containing V sites and thus also V elementary cubes. The number of cubes of branching genus ν is denoted by N_ν, and obviously, $\sum_{\nu=0}^{6} N_\nu = V$. Then the dimensionless branching density (12) can be expressed with Eq. (15) as

$$\begin{aligned}\hat{\rho}_B &= \frac{N_3 + N_5}{V} \\ &= q_B \frac{\sum_{\nu=2}^{6} N_\nu}{V} \\ &= 3q_B \frac{\sum_{\nu=2}^{6} [\nu + (2-\nu)] N_\nu}{6V} \\ &= 3q_B \frac{\sum_{\nu=2}^{6} \nu N_\nu}{6V} \cdot \left\{ 1 - \frac{\sum_{\nu=2}^{6} (\nu-2) N_\nu}{\sum_{\nu=2}^{6} \nu N_\nu} \right\} \\ &= 3q_B \hat{\rho} \lambda \end{aligned} \tag{17}$$

with the dimensionless factor

$$\lambda \equiv 1 - \frac{\sum_{\nu=2}^{6} (\nu-2) N_\nu}{\sum_{\nu=2}^{6} \nu N_\nu} \in [0,1]. \tag{18}$$

In the last step in Eq. (17), we have used the fact that a cube with branching genus ν has ν nontrivial plaquettes on its surface, each of which is shared with an adjacent cube. Thus, the sum $\sum_\nu \nu N_\nu$ counts every nontrivial plaquette twice, and the dimensionless vortex area density Eq. (8) becomes, after averaging over all planes in the 3D slice,

$$\hat{\rho} = \frac{\frac{1}{2}\sum_{\nu=0}^{6} \nu N_\nu}{3V} = \frac{\sum_{\nu=2}^{6} \nu N_\nu}{6V},$$

since a 3D slice with V sites and periodic boundary conditions contains a total of $3V$ plaquettes. After inserting appropriate factors of the lattice spacing in Eq. (17), we obtain the exact relation

$$\rho_B(T) = 3 w_B(T) \rho(T) \lambda(T,a). \tag{19}$$

As indicated, the coefficient λ may depend on the temperature and the lattice spacing, but it must fall in the range [0, 1]. As a consequence, we obtain an exact inequality between physical quantities,

$$\rho_B(T) \le 3 w_B(T) \rho(T), \tag{20}$$

which must be valid at all temperatures. Moreover, the deviation from unity in the coefficient λ can be estimated, from Eq. (18),

$$\begin{aligned}\lambda &= 1 - \frac{\sum_{\nu=2}^{6} (\nu-2) N_\nu}{\sum_{\nu=2}^{6} \nu N_\nu} \\ &= 1 - \frac{N_3 + N_5}{\sum_{\nu=2}^{6} \nu N_\nu} + 2 \frac{N_4 + N_5 + 2N_6}{\sum_{\nu=2}^{6} \nu N_\nu} \\ &= 1 - \frac{1}{6}\frac{\hat{\rho}_B}{\hat{\rho}} + \mathcal{O}\left(\frac{N_4}{N_2}\right) = 1 - \frac{1}{6}\frac{\rho_B(T)}{\rho(T)} a + \mathcal{O}\left(\frac{N_4}{N_2}\right). \end{aligned}$$

Here, the leading correction to unity vanishes in the continuum limit $a \to 0$ since both ρ_B and ρ are physical. Furthermore, the next-to-leading term has the simple branching $\nu = 3$ removed and starts with the probability of self-intersection or osculation, which is small and presumably

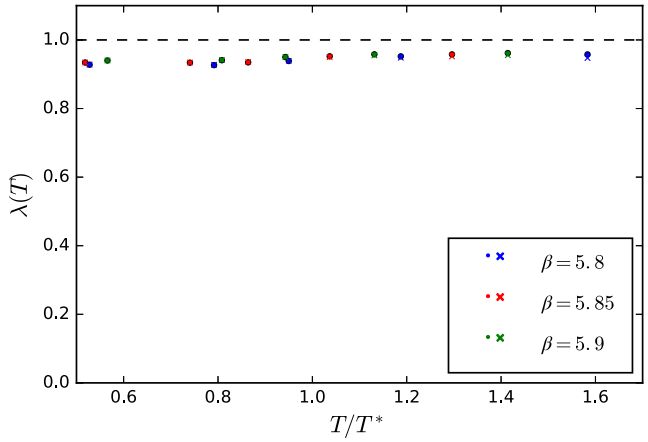

FIG. 7. The ratio λ of physical quantities from Eq. (18). Data comprises all available couplings and temperatures. Statistical errors are generally at the 5% level, but no error bars have been displayed to improve the readability of the plot.

also proportional to a, by the same argument that led from Eq. (15) to Eq. (16) above. Thus, it is conceivable that $\lambda(T, a) = 1 + \mathcal{O}(a)$ and Eq. (19) turns into the relation

$$w_B(T) = \frac{1}{3}\frac{\rho_B(T)}{\rho(T)} \tag{21}$$

for $a \to 0$. This is renormalization group invariant. We have tested this conjecture numerically by computing the relevant coefficient $\lambda(T, a)$ from Eq. (18). The result is presented in Fig. 7, where we accumulate all available data for all temperatures and lattice spacings. As can be seen, λ is indeed in the range $[0, 1]$, independent of temperature and very close to unity. Since the overall statistical uncertainty is about 5% and our calculations were all done at the lower end of the scaling window with a relatively large lattice spacing a, our numerics are at least compatible with $\lambda = 1$ and hence Eq. (21) in the continuum limit. Further calculations with larger and finer lattices are clearly necessary to corroborate this conjecture.

Equation (21) shows that the drop of the branching density ρ_B at the phase transition is *not* due to an overall reduction of vortex matter ρ, since the branching probability per unit length, $w_B \sim \rho_B/\rho$, shows the same qualitative behavior as ρ_B, even after scaling out the overall vortex density. The conclusion is that both the branching point density $\rho_B(T)$ from Eq. (13) and the branching probability $w_B(T)$ per unit length Eq. (16) can be used as a reliable indicator for the phase transition and as a signal for the change in the geometrical order of the vortices at the deconfinement transition. Our findings in full Yang-Mills theory match the general expectations discussed above, and they also comply with the predictions made in the random vortex world-surface model [16].

V. CONCLUSION

In this work, we have studied the probability of center vortex branching within SU(3) Yang-Mills theory on the lattice. The general expectation, confirmed only in models so far, was that the branching probability should be sensitive to the geometry of vortex clusters and thus provide an alternative indicator for the deconfinement phase transition. We were able to corroborate this conjecture: both the branching point density $\rho_B(T)$ and the branching probability per unit length $w_B(T)$ are independent of the lattice spacing and exhibit a steep drop at the critical temperature, though a remnant branching probability remains even above T^*. This effect is much more pronounced in space slices of the original lattice, which clearly indicates a dominant alignment of vortices along the short time direction within the deconfined phase. The same conclusion can be drawn from the renormalization group invariant relation $w_B \sim \rho_B/\rho$, which proves that the drop in the branching density is *not* due to an overall reduction of the vortex matter ρ, but instead, it must be caused by the change in the geometry of the vortex cluster.

In future studies, it would be interesting to directly control the branching of vortices and study its effect on the confinement and the chiral symmetry breaking, e.g., through the Dirac spectrum in the background of such branching-free configurations. The control over vortex branching could also address the obvious conjecture that the different (first) order of the phase transition for $G = \mathrm{SU}(3)$, as compared to the weaker second order transition of $G = \mathrm{SU}(2)$, is a result of the new geometrical feature of vortex branching.

ACKNOWLEDGMENT

This work was supported by Deutsche Forschungsgemeinschaft (DFG) under Contract No. Re 856/9-2.

[1] G. Mack and V. B. Petkova, Ann. Phys. (N.Y.) **125**, 117 (1980).
[2] L. Del Debbio, M. Faber, J. Greensite, and S. Olejnik, Phys. Rev. D **55**, 2298 (1997).
[3] K. Langfeld, H. Reinhardt, and O. Tennert, Phys. Lett. B **419**, 317 (1998).
[4] M. Engelhardt and H. Reinhardt, Nucl. Phys. **B567**, 249 (2000).

[5] H. Reinhardt, Nucl. Phys. **B628**, 133 (2002).
[6] S. M. Hosseini Nejad and M. Faber, J. High Energy Phys. 09 (2017) 068.
[7] S. M. H. Nejad, M. Faber, and R. Höllwieser, J. High Energy Phys. 10 (2015) 108.
[8] R. Bertle, M. Engelhardt, and M. Faber, Phys. Rev. D **64**, 074504 (2001).
[9] J. Gattnar, C. Gattringer, K. Langfeld, H. Reinhardt, A. Schäfer, S. Solbrig, and T. Tok, Nucl. Phys. **B716**, 105 (2005).
[10] R. Hollwieser, M. Faber, J. Greensite, U. M. Heller, and Š. Olejník, Phys. Rev. D **78**, 054508 (2008).
[11] H. Reinhardt and T. Tok, Phys. Rev. D **68**, 065004 (2003); H. Reinhardt, O. Schröder, T. Tok, and V. Ch. Zhukovsky, Phys. Rev. D **66**, 085004 (2002).
[12] E. O'Malley, W. Kamleh, D. Leinweber, and P. Moran, Phys. Rev. D **86**, 054503 (2012).
[13] K. Langfeld, O. Tennert, M. Engelhardt, and H. Reinhardt, Phys. Lett. B **452**, 301 (1999); M. Engelhardt, K. Langfeld, H. Reinhardt, and O. Tennert, Phys. Rev. D **61**, 054504 (2000).
[14] L. E. Oxman and H. Reinhardt, Eur. Phys. J. C **78**, 177 (2018).
[15] M. Engelhardt and H. Reinhardt, Nucl. Phys. **B585**, 591 (2000).
[16] M. Engelhardt, M. Quandt, and H. Reinhardt, Nucl. Phys. **B685**, 227 (2004).
[17] M. Quandt, H. Reinhardt, and M. Engelhardt, Phys. Rev. D **71**, 054026 (2005).
[18] K. Langfeld, Phys. Rev. D **69**, 014503 (2004).
[19] Ph. de Forcrand and M. D'Elia, Phys. Rev. Lett. **82**, 4582 (1999).
[20] N. Cabibbo and E. Marinari, Phys. Lett. **119B**, 387 (1982).
[21] J. E. Mandula and M. Ogilvie, Phys. Lett. B **248**, 156 (1990).
[22] V. Bornyakov, D. Komarov, and M. Polykarpov, Phys. Lett. B **497**, 151 (2001).
[23] T. Kovacs and E. Tomboulis, Phys. Lett. B **463**, 104 (1999).
[24] A. Sternbeck, E.-M. Ilgenfritz, M. Müller-Preussker, and A. Schiller, Phys. Rev. D **72**, 014507 (2005).
[25] G. Burgio, M. Quandt, and H. Reinhardt, Phys. Rev. Lett. **102**, 032002 (2009); G. Burgio, M. Quandt, H. Reinhardt, and H. Vogt, Phys. Rev. D **95**, 014503 (2017).
[26] B. Lucini, M. Teper, and U. Wenger, J. High Energy Phys. 01 (2004) 061.
[27] G. S. Bali, K. Schilling, J. Fingberg, U. M. Heller, and F. Karsch, Int. J. Mod. Phys. C **04**, 1179 (1993).